Network reorganisation reveals somato-motor transition from segregation to integration during tonic pain

Network reorganisation reveals somato-motor transition from segregation to integration during tonic pain

Wenxin Su[a,b], Chris G. Antonopoulos[b], Elia Valentini[a,*]

Abstract

The sustained nature of tonic pain makes it a useful experimental analogue for studying the prolonged neural processing involved in chronic pain. However, research is yet to identify its consistent and generalisable biomarkers. Here, we analysed electroencephalography data recorded in 36 volunteers during 5-minute sessions of noxious hot and innocuous warm water immersion using network-based statistics and graph theory-based analysis. Our results revealed a brain-wide reorganisation of functional connectivity during tonic pain, marked by a global shift from segregation to integration. This shift was characterised by a transition from intra- to internetwork communication, with the Somato-Motor (SomMot) network playing a pivotal role. During innocuous warmth, the SomMot network exhibited significantly higher functional specialisation for localised sensory processing. During noxious heat, however, it shifted to an integrative coordinator, a finding reinforced by a significant discrepancy in global clustering coefficient when intranetwork connections were excluded. We also found that psychological traits modulated global network inferences (GNIs) in distinct, clinically relevant ways: pain catastrophising was positively associated with network segregation and integration during pain, whereas anxiety was negatively associated with segregation and integration during innocuous warmth. Notably, a machine learning model using these GNIs achieved 86% accuracy in classifying noxious heat from innocuous warmth. Together, our findings elucidate the transformation from segregated processing to integrated network dynamics induced by tonic pain, characterised by a transition in the SomMot network functioning as an integrator. Critically, global network inferences may serve as valuable predictors of pain experiences, highlighting their translational potential in pain neuroscience.

Keywords: Tonic pain, EEG, Graph theory, Somato-motor network, Internetwork connectivity, Machine learning, Biomarker, Classification

1. Introduction

Identifying reliable biomarkers for chronic pain remains a major challenge because of reliance on self-reports, clinical heterogeneity, and the engagement of multiple brain systems.[9,61,68] Functional magnetic resonance imaging (fMRI) studies have consistently implicated several large-scale brain networks in pain processing, with central roles for the somato-motor (SomMot), frontoparietal, and dorsal attention networks.[31] For instance, sustained myofascial pain has been associated with a shift in contralateral primary sensorimotor connectivity toward the salience network,[21] whereas capsaicin-induced pain increases crosstalk among SomMot, default mode, auditory, and visual networks.[38]

[a] *Department of Psychology and Centre for Brain Science, University of Essex, Colchester, United Kingdom,*

[b] *School of Mathematics, Statistics and Actuarial Science (SMSAS), University of Essex, Colchester, United Kingdom*

**Corresponding author. Address: Department of Psychology, University of Essex, Wivenhoe Park, Colchester CO4 3SQ, United Kingdom.. E-mail address: evalent@essex.ac.uk (E. Valentini).*

Electroencephalography (EEG) studies further highlight the involvement of alpha band oscillations in tonic pain. During sustained heat pain, alpha power in sensorimotor areas is suppressed, whereas phase-based alpha connectivity between sensorimotor and medial prefrontal cortex increases.[44] These effects are thought to originate from the sensorimotor cortex[47,63] and have been showed to correlate negatively with pain ratings.[47,48] Together, these findings suggest that the SomMot network contributes to both intranetwork (local) and internetwork (distributed) coordination during tonic pain, possibly mediated by alpha-band dynamics.

Graph theory provides a powerful framework to quantify such brain network organisation. Nodes represent brain regions, and edges reflect functional connectivity, allowing computation of global network inferences (GNIs) to quantify graph properties, which capture the balance between segregation (eg, global clustering coefficient [Gcc]) and integration (eg, global efficiency [Geff]) in brain function.[4,52] Notably, classification analyses using a combination of GNIs from alpha-band EEG have achieved up to 92% accuracy in differentiating pain from no-pain states,[40] emphasizing their translational promise.

However, a systematic review indicated that although GNI differences exist between patients with chronic pain and healthy controls, the findings remain mixed.[33] Similarly, experimental pain studies report conflicting results. Some fMRI studies have reported increased Gcc and reduced small-worldness (Sw) and modularity (Mod) in response to noxious stimuli.[15,51,69] In

contrast, even in the same EEG dataset, no significant Gcc or Geff differences were observed when using phase-locking value, whereas significant Gcc increases during pain emerged using the debiased weighted phase lag index (dwPLI).[44]

To address these discrepancies, we aimed to analyse brain-wide graphs, higher-order intra-SomMot, and internetwork graphs. By combining functional connectivity topology with graph-theoretical analyses, we sought to provide insights into the pain-induced brain reorganisation. Given that baseline neural activity normalisation may reduce intersubject variability, thereby unmasking condition-specific network properties, we also assessed its influence by both relative and absolute comparisons (see Methods). Finally, we explored the predictive utility of GNIs for classifying pain states.

To achieve these goals we reanalysed a secondary EEG dataset recorded during a tonic thermal pain model.[60] We hypothesised that tonic pain would determine the reorganisation of functional connectivity from intranetwork segregation to internetwork integration, with the SomMot network playing a central role. In addition, we expected that combined GNIs would exhibit robust predictive power in classifying pain states.

If validated, these EEG-based biomarkers could contribute to the development of objective pain assessment tools, particularly for noncommunicative individuals and chronic pain populations.

2. Methods

2.1. Participants

Forty-three participants volunteered for the study. Seven participants were excluded: one had taken a painkiller before the experiment, another failed the perceptual matching procedure (detail in experimental procedure), and data from the 5 were excluded because of technical issues with EEG recording. Therefore, only 36 were analysed and 22 of these were female, with a mean age of 25.36 years (range: 20-56 years). All participants had normal or corrected-to-normal vision and normal hearing. Before attending, the volunteers were asked to complete a questionnaire to ensure that they had no history of neurological, psychiatric, or pain disorders that could interfere with the study or jeopardise their safety. Psychological traits relevant to pain processing were also assessed using the Pain Catastrophising Scale (PCS)[56] and the trait component of the State-Trait Anxiety Inventory (STAI).[57] These measures were later included in correlational analyses.

The study received approval from the Ethics Committee of the University of Essex (EV1801).

2.2. Experimental procedure

We used a 30-L water tank (RW-3025P, Medline Scientific, Rotherham, United Kingdom) to deliver 2 out of 3 experimental sensory conditions. We induced an experience of tonic pain by having participants immersing their left hand in hot water at 44.50 (±0.49)°C, referred to as the hot condition. The starting temperature (45°C) was selected based on previous studies,[13,17] which found it to induce a moderate level of pain. We induced an innocuous warm sensation by reducing the water temperature by 6°C less than the hot condition. During the stimulation, participants were asked to rate their level of unpleasantness every 10 seconds using an onscreen visual analogue scale (VAS), with verbal anchors at 0 ("No unpleasantness") and 100 ("Intolerable unpleasantness"). In total, participants provided 30 ratings for each condition. At the beginning and end of the experimental session, both eyes-open and eyes-closed resting-state sessions were recorded, each lasting about 2.5 minutes. Hence, each condition lasted around 5 minutes. Data from the resting-state eyes-open condition only were included in this study. The third sensory condition (ie, tonic sound) is not included in the current study (see 60 for the full experimental design).

Before the experiment, all participants were required to complete a perceptual matching procedure. This critical step ensured the subjective unpleasantness of the auditory stimulus was equivalent to that of the painful heat stimulus for each participant. This matching was a cornerstone of the original experimental design. For consistency, we did not include the single participant who failed the procedure in the seminal study within the current reanalysis. Because the target unpleasantness rating ranged from 50 to 75 on the VAS (0-100), this confirmed that we successfully induced a moderate level of unpleasantness during the hot stimulation. If the unpleasantness rating for the warm stimulation was significantly lower than that for the hot stimulation, it would further support the success of the thermal manipulation. Moreover, if unpleasantness increased during the hot water immersion, it would provide additional evidence for the successful induction of tonic pain in our study.

2.3. Electroencephalography preprocessing

Electroencephalography data were recorded using an electrode montage of 62 channels consisting of all 10 to 20 system electrodes with Ag/AgCI electrodes (Easycap, BrainProducts GmbH, Gilching, Germany). The impedance of all electrodes was kept below 10 kΩ, and the EEG signal was amplified and digitised at 1000 Hz. The online reference was placed upon the left earlobe, and the ground was located at electrode position AFz.

The EEG data in hot, warm, and resting-state open-eyes conditions before stimulation were preprocessed using a high-pass value set to 0.1 Hz and the low-pass value set to 100 Hz. All data were down sampled to 500 Hz. Artefacts such as eye-blinking and muscle movements were removed using independent component analysis (ICA).

After ICA, the data were further denoised with a notch filter to exclude the frequency bands from 49.5 to 50.5 Hz, were re-referenced to the average of all electrodes,[12] and were segmented into 2-second epochs with a 25% overlapping rate and 25% baseline correction.

2.4. Analytical design

All analyses were performed in MATLAB using the EEGLAB toolbox,[8] FieldTrip toolbox,[45] the Brain connectivity toolbox,[53] the DISCOVER-EEG toolbox,[11] the Network-Based Statistic toolbox V1.2 (https://www.nitrc.org/projects/nbs/), and custom-written scripts.

Preprocessed data were analysed using the pipeline showed in **Figure 1**. The brain-wide graph (**Fig. 1A**) was constructed in both sensor and source spaces. In the sensor space, we focused on the alpha band, whereas exploratory analyses were also conducted in other frequency bands. We assessed functional connectivity using dwPLI, and the thresholded matrices were binarised using 1 standard deviation above the median for each subject's connectivity matrix in each condition to create adjacency matrices for subsequent network-based statistics (NBS) and graph analyses. The source space data were reconstructed into 100 regions of interest of the Schaefer atlas[55] using an atlas-based beamforming approach via the Discover EEG toolbox. Further analysis based on brain-wide graph (**Fig. 1B**) for intra- and internetwork connections was conducted

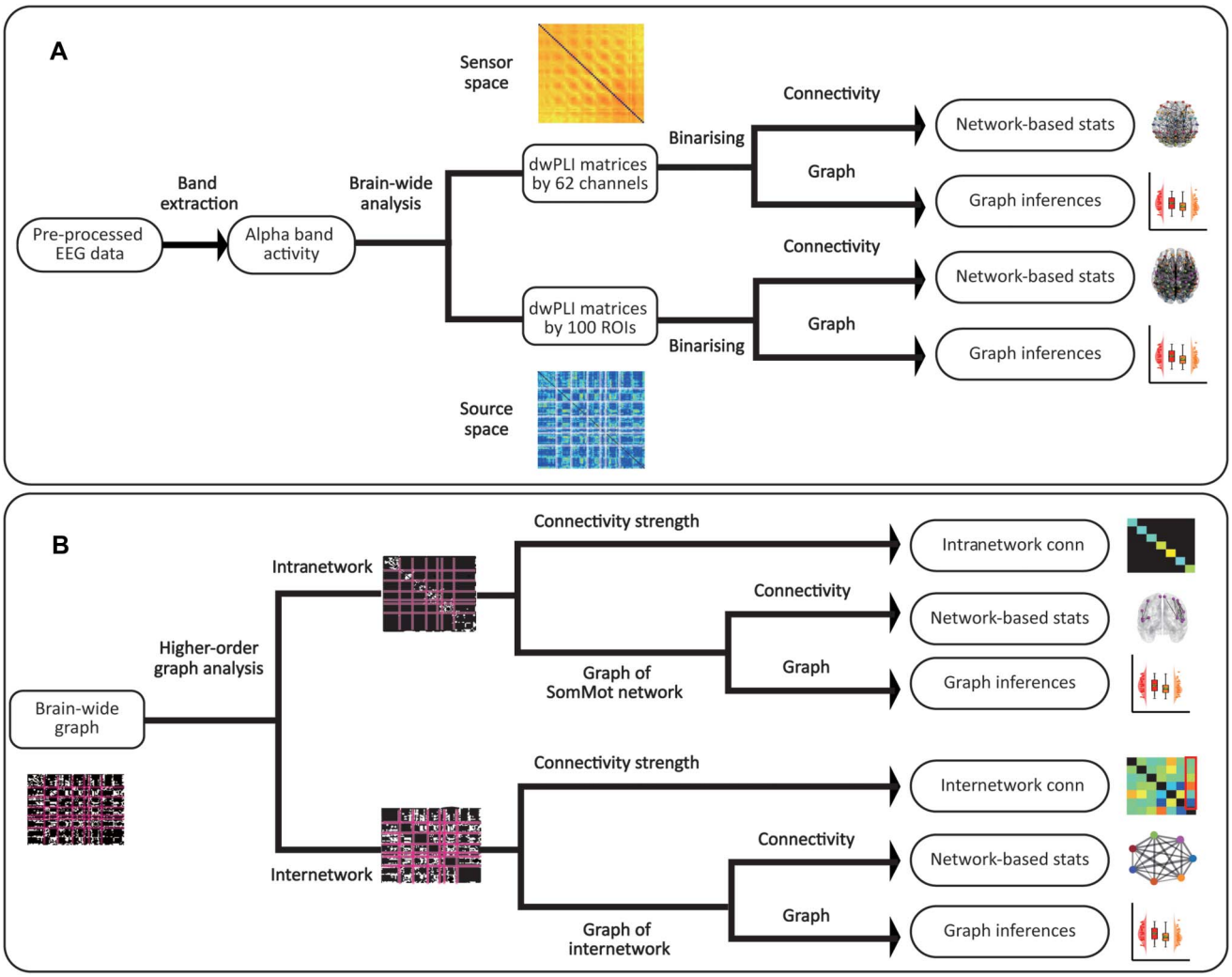

Figure 1. Pipeline for the analysis of EEG data. (A) The preprocessed EEG data were extracted in the alpha band and then used for the brain-wide functional connectivity assessment using dwPLI in both sensor and source spaces. The functional connectivity matrices were binarised using a threshold of one standard deviation above the median for each subject's connectivity matrix in each condition and then analysed through NBS and graph analysis. (B) The brain-wide graphs in the source space were further constructed as a higher-order graph involving 7 networks in parcellation. For intranetwork analysis, statistical comparisons of the intranetwork connectivity strength were conducted, and the binarised graph of the SomMot network was analysed using NBS and graph analysis. For internetwork analysis, statistical comparisons of the mean internetwork connections between each pair of networks were conducted, and internetwork connections between pairs of networks were constructed as weighted matrices and analysed through NBS, as well as both local and global graph analyses. Conn, connectivity; dwPLI, debiased weighted phase lag index; EEG, electroencephalography; NBS, network-based statistics; ROI, regions of interest; SomMot, somato-motor; stats, statistics.

in the source space, using the 100-region atlas that classifies 7 networks. Intranetwork connections for all 7 networks were analysed, with particular focus on the binary SomMot network. In addition, internetwork connections were evaluated using weighted matrices, using NBS and graph theory. Detailed methodology is provided in Section 2.5, 2.6 and the supplementary material, http://links.lww.com/PAIN/C435.

We performed absolute and relative comparisons between the hot and warm conditions in both spaces. Specifically, the functional connectivity matrices for the relative comparisons were calculated by dividing the original dwPLI for each sensory condition by the dwPLI of the prestimulation resting-state eyes-open condition for each participant (we excluded the closed eye condition for this purpose based on the assumption that the open eyes resting state would have provided a better reference baseline for sensory-related mental states).

Notably, NBS-based graphs revealed connectivity patterns for group-level contrasts between hot and warm stimulation. In parallel, the graph-theoretical analysis was performed on individual-level connectivity matrices to compute several network inferences, which were then submitted to group-level statistical testing to identify condition-dependent alterations in graph characteristics. Although these 2 analytical approaches are methodologically distinct, they provide complementary insights: NBS highlights condition-contrast connectivity patterns, whereas graph-theoretical inferences quantify the corresponding network-level properties.

2.5. Methodological rationale for dual analytical approach: absolute and relative comparison

In this study, we used both absolute and relative comparison methods throughout the analysis, based on methodological and theoretical considerations rather than as a duplication of analyses.

The use of resting-state baseline normalisation is a well-established methodological approach in neuroimaging research,

used to enhance the detection and interpretation of condition-specific neural dynamics. This technique improves both the specificity and sensitivity of findings. For example, Alain et al.[3] demonstrated enhanced specificity by using baseline-referenced analyses to dissociate overlapping activations during pitch and spatial auditory tasks, revealing distinct neural pathways that were otherwise conflated. Similarly, the utility of normalisation for sensitivity is evident in clinical neurophysiology. Feng et al.[10] showed that a normalised alpha power metric, but not the absolute power, successfully uncovered a significant correlation with clinical pain intensity in patients with chronic low back pain. Together, these examples demonstrate that relative, normalised comparisons are vital for revealing subtle, condition-specific neural associations which absolute measures may obscure, thus supporting our analytical approach.

In the present study, we implemented both absolute and relative analyses for complementary reasons. Absolute measurements of functional connectivity are widely used but can be strongly influenced by intersubject variability in baseline neural activity. Relative comparisons help to mitigate this variability, thereby unmasking condition-specific network properties that may otherwise be obscured. This dual approach allowed us to examine network dynamics from two perspectives: an absolute measure of overall connectivity strength, and a relative measure that highlights within-subject changes relative to baseline.

Furthermore, implementing both analytical approaches allowed us to evaluate the robustness of our findings across different methodological frameworks. The convergence of patterns across the 2 approaches increases confidence that the observed effects reflect genuine condition-specific network. Although this strategy adds analytical complexity, we believe it strengthens the methodological rigour of the study and the validity of its conclusions.

2.6. Brain-wide graph analysis

We conducted a brain-wide graph analysis in both sensor and source spaces (**Fig. 1A**). In the analysis of sensor space, we extracted the preprocessed EEG data in the alpha band (8-13 Hz) using the Hilbert transform. To estimate functional connectivity in phase synchronisation, we performed further analysis (details in the supplementary materials, http://links.lww.com/PAIN/C435) using the dwPLI[6] because of its significant reduction of volume conduction effects.[46]

For each participant and condition, dwPLI values were computed for all pairs of 62 EEG channels and averaged across epochs to construct functional connectivity matrices. These matrices were then binarised using a threshold set at 1 standard deviation above the median of each matrix. The resulting binarised undirected adjacency matrices were used for subsequent connectivity and graph analyses.

2.6.1. Connectivity analysis for sensor space graphs

Connectivity analysis was performed using the NBS toolbox[66,67] to identify significant differences in brain connectivity between conditions. Network-based statistics, a nonparametric statistical approach, uses cluster-based analysis while controlling for family-wise error rate.[67] In the sensor space, we applied NBS to compare the 2 conditions using 62 $\times$ 62 node graphs.

2.6.2. Analysis for source space graphs

In the source space analysis, we projected the preprocessed sensor space data onto 100 regions of interest from the Schaefer atlas[55] using an atlas-based beamforming approach via the Discover EEG toolbox.[11] We computed dwPLI matrices for each participant and condition and then binarised them into adjacency matrices using the same thresholding procedure applied in the sensor space analysis. Graphs comprising 100 nodes were then constructed, and connectivity and graph-theoretical analyses were performed following the same procedures as in the sensor space.

2.7. Higher-order graph analysis

Based on the binarised source space graphs, we further analysed higher-order graphs (**Fig. 1B**), which included 7 functional networks: Visual (Vis), Somato-motor (SomMot), Dorsal Attention (DorsAttn), Salience-Ventral Attention (SalVentAttn), Limbic, Control (Cont), and Default.

2.7.1. Intranetwork analysis

For the intranetwork analysis, only the intranetwork connections within each of the 7 networks were retained. The connectivity strength was calculated by averaging these connections and then compared between the 2 conditions.

Apart for the intranetwork connectivity analysis, a focussed analysis was conducted on the SomMot network. Brain regions corresponding to the SomMot network were extracted, yielding a 14 $\times$ 14 binarised, undirected subgraph. Connectivity and graph-theoretical analyses were then performed using the same procedures as those applied in the sensor and source spaces.

2.7.2. Internetwork analysis

For the internetwork analysis, all the connections between different networks were preserved, whereas intranetwork connections were excluded. For each network, internetwork connectivity strength was calculated as the average of its connections with the other 6 networks.

We also applied connectivity and graph analysis on the resulting 7 $\times$ 7 weighted internetwork graphs. Given the limited number of nodes in the higher-order graph, 2 GNIs were computed: Gcc and Geff. In addition, 2 local inferences were assessed for each node (network) in the internetwork graph: edge betweenness centrality (Ebc) and local clustering coefficient (Lcc).

2.8. Graph analysis based on graph theory

Graph analysis consisted of 4 GNIs in the sensor space, source space, and intranetwork graphs: Gcc, Geff, Sw, and Mod. Global clustering coefficient is one of the best-known indicators of functional segregation, quantified as the average clustering coefficient of each node in the graph. Clustering coefficients at the node level indicate the fraction of the node's neighbours that are also neighbours of each other.[64] A high fraction of triangles in the graph implies functional segregation, reflecting the brain's ability to use densely interconnected regions to sustain specialised brain processes. Global efficiency is a measure of functional integration,[1] facilitating the rapid exchange of information across distributed brain regions. It is computed as the average inverse shortest path length, which is the minimum number of edges required to connect any pair of nodes in a graph.[30] Small-worldness describes how a graph is more clustered than random networks with similar characteristic path lengths.[64] It is calculated as the ratio of the clustering coefficient

to Geff compared to random networks. Small-world organisation reflects an optimal balance of functional integration and segregation.[58] Mod quantifies the degree to which a graph can be subdivided into clearly delineated groups.[41] Unlike other network-structure measures, Mod relies heavily on optimisation algorithms that subdivides the graph into nonoverlapping modules. We used the maximised Mod algorithm,[42] which is an accurate and sufficiently fast approach to quantify Mod for smaller networks.[52] Higher Mod values indicate that a network has a stronger community structure, meaning there are dense connections among nodes within the same module (or group) and sparser connections between nodes in different modules. This suggests that the network is more efficiently organised into distinct subgroups, which can enhance functional specialisation and improve resilience to disruptions.

It is worth noting that segregation in brain-wide and intranetwork graphs reflects functional specialisation within a given graph, whereas integration characterises global information flow. However, when within-network connectivity is excluded, the local network inferences derived from higher-order internetwork graphs represent dynamics related to interaction with other networks. In this context, GNIs primarily capture internetwork communication.

2.9. Statistical analysis

All statistical comparisons, except for the network-based statistics (as implemented in the NBS toolbox), were conducted using IBM SPSS (version 20; IBM Corp, Armonk, NY). Detailed NBS statistics and visualisation methods are in the supplementary materials, http://links.lww.com/PAIN/C435.

For the graph analysis, we used different statistics for global and local network inferences. For GNIs in all graphs, we applied 2-way repeated measures analysis of variance (ANOVA), followed by post hoc comparisons using Bonferroni-corrected 2-sided paired sample *t*-tests with an alpha level set at 0.05. Using ANOVA, we not only assessed the differences between 2 conditions but also examined how these differences varied between absolute and relative comparison methods. As for the local network inferences, which were conducted exclusively in higher-order internetwork graphs, we computed paired-sample *t*-tests for Lcc, with an alpha level set at 0.05 (2-tailed) with false discover rate (FDR) correction for multiple comparisons. As for Ebc, we also performed the NBS to identify significant differences in edge-level centrality. To analyse the connectivity strength within intra- and internetwork graphs, we performed 2-tailed paired-sample *t*-tests with an alpha level set at 0.05, with FDR correction for multiple comparisons between conditions under both absolute and relative comparison methods.

2.10. Correlation analysis between global network inferences and self-report data

Before classification analyses, we quantified the correlation between GNIs and behavioural ratings for hot and warm conditions separately. To assess the potential influence of age, we conducted correlations between participant age and each GNI. We further evaluated how individual differences in pain responsiveness modulated GNIs using partial correlations, controlling for age and sex. Individual differences were defined using 4 behavioural measures: pain perception was defined as the mean difference in unpleasantness ratings between hot and warm conditions for each participant; pain tolerance was operationalised as the change in average unpleasantness rating from the first third to the last third of the hot stimulation period; and pain-related psychological traits were assessed using the PCS and the trait component of the STAI.

2.11. Machine learning classification

Global network inferences were selected as features for classification, derived from individual or combined graph types including sensor space, source space, intra-SomMot, and internetwork graphs under both absolute and relative comparison methods. Our feature inclusion was primarily theory-driven rather than performance-optimised, as the goal was to use classification to test the robustness of GNIs as potential biomarkers. We incorporated all GNIs from 4 graph types because each was hypothesised to capture distinct aspects of brain network organisation that may differentiate responses to hot and warm stimuli. Given the modest sample size, we deliberately avoided data-driven feature selection methods, which could increase the risk of overfitting and compromise the validity of cross-validation. Instead, we systematically evaluated all possible combinations of the 4 feature sets and reported the 3 best-performing combinations. This strategy ensured methodological transparency and reduced the risk of overfitting by avoiding any optimisation on the test set.

To assess the predictive capacity of GNIs in distinguishing tonic pain states (hot vs warm), we implemented a linear support vector machine (SVM) with L2 regularisation. The regularisation parameter (λ) was automatically optimised within each training fold. Input features (GNIs) were standardised using z-score normalisation based on the training set's mean and standard deviation, and the trained model was used to classify the held-out subject's data.

A leave-one-subject-out cross-validation framework was applied across all 36 participants. For each fold, 1 subject's data were held out for testing, whereas the remaining data were used for training and normalisation. Model performance was evaluated using area under the receiver operating characteristic curve (AUC-ROC), and pooled inferences from the confusion matrix, including accuracy, sensitivity, and specificity.

To assess the significance of the classifier's discriminative performance, we conducted a permutation test with 1000 iterations. For each iteration, participant labels were randomly shuffled to disrupt the true feature-label relationship, and the entire cross-validation pipeline was repeated using these permuted labels. The null distribution of AUC-ROC values was generated from these shuffled-label iterations. The empirical *P*-value was computed as the proportion of permutation AUCs exceeding or matching the original model's AUC. This approach quantifies the probability that the observed classification performance occurred by chance under the null hypothesis of no true feature-label association.

3. Results

3.1. Perception

As we already showed in a previous study,[60] the unpleasantness ratings were significantly different between tonic hot and warm stimulation ($T[35] = 36.31$, $P_{FDR} < 0.001$). This difference was accounted for by greater unpleasantness during the hot condition (hot: 67.83 ± 9.18, 95% CI = [64.73, 70.94]; warm 3.17 ± 1.30, 95% CI = [2.23, 6.93]). These results demonstrate that the manipulation of thermal stimulation was effective in inducing distinctive affective states in healthy participants. Moreover, a paired-sample *t* test comparing the average unpleasantness

rating from the first third of the hot condition to the average rating from the last third revealed a significant increase (t [35] = 5.55, $P < 0.001$), suggesting a trend of sensitisation to the stimulus over time within the hot condition and thereby validating the successful experimental manipulation of tonic pain in our study.

3.2. Brain-wide graph results in sensor space

3.2.1. Sensor space connectivity results

In the absolute comparison (**Fig. 2A**), the group-level graph construction in the axial plane revealed that edges in the hot condition were clustered bilaterally from the central to parietal regions and within parietal areas (**Fig. 2A** third row left panel). In contrast, the warm condition exhibited a more distributed edge pattern within brain regions, indicated by nodes of the same colour (**Fig. 2A** third row right panel). Network-based statistics revealed a significant graph with larger connectivity in the hot condition relative to warm condition (**Fig. 2A** fourth row left panel), comprising 60 nodes and 378 edges, predominantly distributed in posterior regions ($P < 0.001$). Conversely, the warm condition (**Fig. 2A** fourth row right panel) yielded a significant graph with larger connectivity relative to hot condition, consisting of 62 nodes and 410 edges, with a concentration of connections in the central region ($P < 0.001$). The relative hot and warm conditions displayed distinct differences in both the dwPLI matrices and the adjacency matrices (**Fig. 2B**). Connections were generally distributed throughout the scalp in the group-level relative hot graph (**Fig. 2B** third row left panel), with a greater concentration in the anterior regions, whereas the relative warm condition displayed a more central distribution (**Fig. 2B** third row right panel). The relative hot condition demonstrated significantly greater connectivity pattern than the relative warm condition (**Fig. 2B** fourth row left panel) with connections predominantly extending from the frontal to parietal regions, comprising 51 nodes and 213 edges ($P < 0.001$). Conversely, the graph for the relative warm condition (**Fig. 2B** fourth row right panel), which indicated significant graph with connectivity larger than the hot condition, revealed a distribution pattern clustered from the frontal-central to central-parietal regions, maximally expressed in the central region, and comprised 58 nodes and 185 edges ($P < 0.001$).

Results from both comparison methods revealed a significant pattern of increased frontoparietal connectivity in the hot condition compared to the warm condition, whereas the warm condition showed a significant stronger connectivity localised in the centre of the scalp relative to the hot condition.

Although the adjacency matrices (**Fig. 2**, second row) and derived graphs (**Fig. 2**, third row) appear markedly different between the absolute and relative comparison methods, this difference reflects a key methodological point. Absolute comparison method captures overall connectivity strength, incorporating both intrinsic baseline activity and task-induced signals, whereas relative (baseline-normalised) matrices diminish shared baseline activity to isolate condition-specific neural responses. Importantly, despite these visual differences at the group level, the condition-contrasts derived from network-based statistics (p-graphs) were more consistent across the 2 methods, suggesting that condition-contrast connectivity patterns were robustly identified regardless of comparison methods used.

3.2.2. Sensor space graph analysis results

Significant main effects of stimulus condition (warm vs hot) and comparison method (absolute vs relative) were observed across all GNIs: functional segregation (Gcc), integration (Geff), small-worldness (Sw), and modularity (Mod) (**Fig. 2C**). Warm stimulation consistently enhanced functional segregation compared to hot stimulation under both comparison methods. Absolute comparisons amplified this effect, yielding higher Gcc than relative methods across stimuli. For functional integration (Geff), relative comparisons produced substantially higher values than absolute methods in both conditions; notably, hot stimulation elicited greater Geff than warm stimulation only in the absolute comparisons. Both Sw and Mod were markedly elevated in the absolute versus relative comparisons, with warm stimulation further increasing Mod in absolute (but not relative) contexts. Detailed statistical results (ANOVA, post-hoc tests) are provided in Supplementary Table 1, http://links.lww.com/PAIN/C435. In summary, graphs induced by warm stimulation showed significantly greater segregation (Gcc), reduced integration (Geff), and improved information transfer into distinct modules (Mod) compared to those elicited by hot stimulation in absolute comparisons. Whilst relative comparisons only reflected increased segregation (Gcc) for warm stimuli.

3.2.3. Exploratory results of graphs derived from theta, beta, and gamma bands in sensor space

Aligned with the alpha band findings, condition-contrast graphs across all frequency bands exhibited greater consistency than group-level condition-specific graphs elicited by hot and warm stimulation (Fig. S1, http://links.lww.com/PAIN/C435). Under absolute comparisons, condition-specific graphs showed predominantly occipital connectivity across all bands (Fig. S1 ABC, http://links.lww.com/PAIN/C435, upper and left-half panel), accompanied by additional frontal connectivity in the theta band (Fig. S1A, http://links.lww.com/PAIN/C435), central connectivity in the beta band (Fig. S1B, http://links.lww.com/PAIN/C435), and prefrontal connectivity in the gamma band (Fig. S1C, http://links.lww.com/PAIN/C435). In contrast, relative comparisons consistently revealed dense right-frontal to left-parietal connectivity across all frequency bands (Fig. S1 ABC, http://links.lww.com/PAIN/C435, upper and right-half panel).

Most condition contrasts did not reach statistical significance, and the corresponding *t*-graphs consisted of sparse connectivity (Fig. S1 ABC, http://links.lww.com/PAIN/C435, lower panel). The only statistically significant contrast was identified in the beta band under absolute comparison (Fig. S1B, http://links.lww.com/PAIN/C435, lower panel second column), which showed greater connectivity during warm than hot stimulation ($P = 0.04$). This graph comprised 107 edges and 52 nodes, distributed within the right hemisphere (frontal to parietal regions) and included cross-hemispheric connections from left frontal to right parietal areas.

Unlike the robust findings in the alpha band, no main effect of stimulus condition was observed in other frequency bands. A post hoc difference was detected only in the theta band, with higher Mod during hot compared to warm stimulation.

Overall, the limited number of significant GNI results and the sparsity of condition-contrast *t*-graphs restrict the interpretability of findings outside the alpha band. Although oscillatory activity in theta, beta, and gamma bands is implicated in pain-related brain dynamics, the present results highlight alpha oscillations as the primary frequency band of interest for subsequent analyses.

The results of GNIs in other frequency bands were shown in Supplementary Table 2, http://links.lww.com/PAIN/C435.

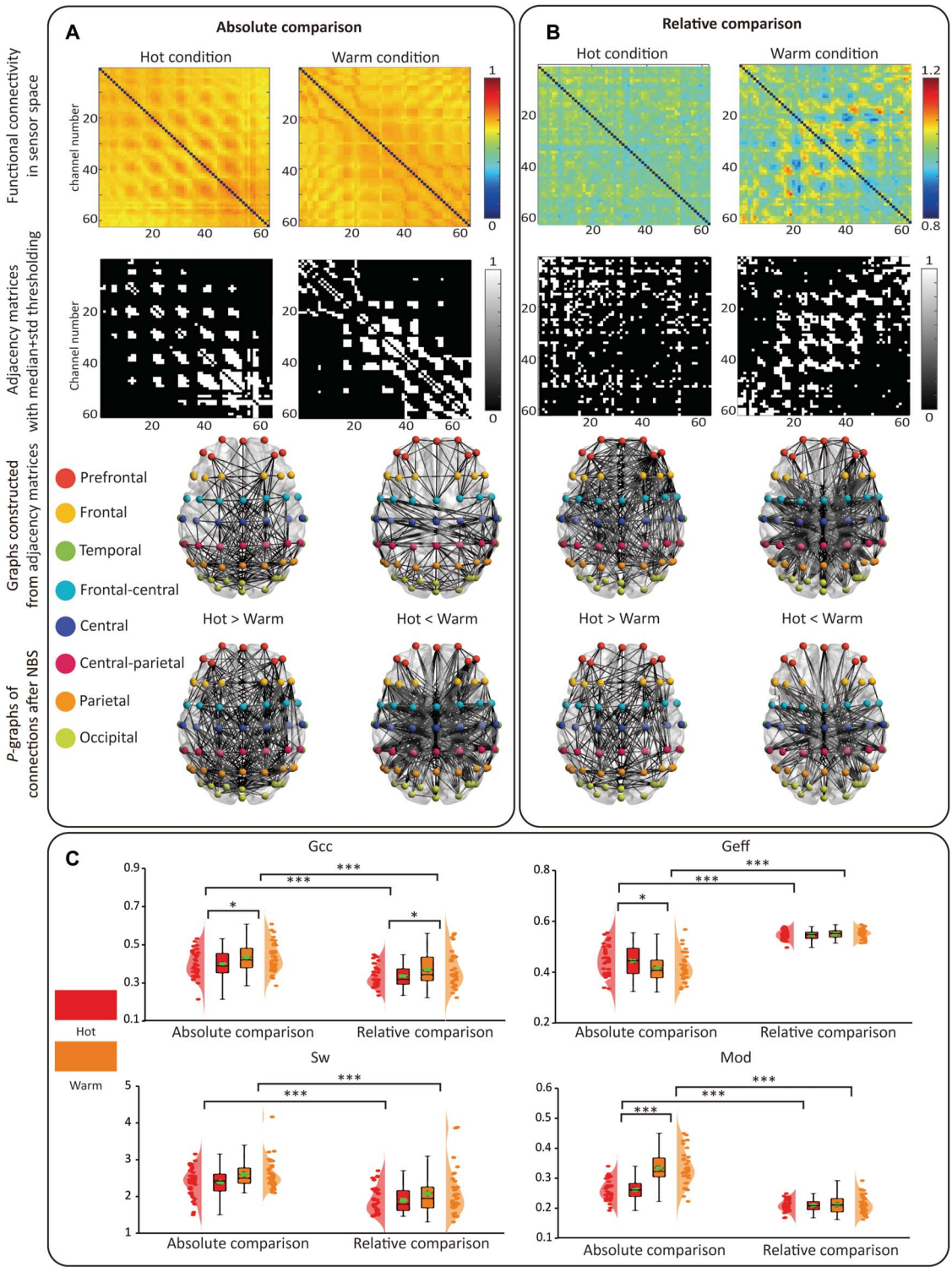

Figure 2. Functional graphs elicited by hot and warm stimulation using 2 comparison methods in sensor space. (A) Group-level functional connectivity matrices for hot and warm stimulation (first row). The corresponding adjacency matrices (second row) were used to construct undirected, unweighted graphs (third row). Sensors corresponding to different scalp regions (Prefrontal, Frontal, Temporal, Frontal-central, Central, Central-parietal, Parietal, and Occipital) were colour-labelled for visual distinction. Condition contrast significant connectivity patterns were identified using NBS and visualised as *P*-graphs (fourth row). The left panel showed hot-preferred responses, and the right panel showed warm-preferred responses. (B) Similar to (A) but using a relative comparison method in which each subject's dwPLI matrix under stimulation was normalised by their own eyes-open resting-state dwPLI matrix. (C) Violin plots with overlaid scatter and box plots show the results of repeated-measures ANOVA with Bonferroni correction for post hoc comparisons of 4 GNIs across the hot (red) and warm (orange) conditions and 2 comparison methods. A green-filled circle with a black edge denotes the mean value for each group. A significant graph emerged, characterised by increased frontoparietal connectivity for hot stimulation, whereas the warm stimulation condition showed stronger, centrally distributed connectivity. In addition, a notably higher degree of functional segregation was observed in the graphs elicited by warm stimulation compared to those from hot stimulation, as demonstrated by both comparison methods. $^{*}P < 0.05$, $^{***}P < 0.001$. Gcc, global clustering coefficient; Geff, global efficiency; GNIs, global network inferences; Mod, modularity; NBS, network-based statistics; Sw, small-worldness.

3.3. Brain-wide graph results in source space

3.3.1. Source space connectivity results

Across both comparison methods (**Figs. 3A and B**), the hot condition graphs displayed a more bilateral distribution (**Figs. 3A and B** third row left panel), whereas the warm condition graphs exhibited a connectivity pattern dominated by the right hemisphere (**Fig. 3A** third row right panel). Although no significant graphs were identified after NBS, *t*-graphs from both comparison methods consistently showed that the hot contrasts were primarily concentrated in the left frontoparietal regions (**Figs. 3A and B**, fourth row, left panel). Conversely, the warm contrasts were predominantly localised in the right hemisphere, particularly around the SomMot networks (**Figs. 3A and B**, fourth row, right panel).

Despite the lack of statistical significance, these results consistently revealed distinct ipsilateral-dominant differential connectivity patterns emerged in brain regions preferentially responsive to hot and warm stimulation consistent across comparison methods (**Figs. 3A and B**, fourth row). Furthermore, source space projections exhibited greater concordance between the absolute and relative comparison methods, particularly in the group-level condition-specific and condition-contrast graphs, than was observed in sensor space analyses.

3.3.2. Source space graph analysis results

In source space, GNIs revealed significant effects of comparison method and stimulus condition (**Fig. 3C**). Absolute comparison consistently produced higher functional segregation (Gcc) than relative comparison across both stimulus conditions, whereas warm stimulation increased Gcc specifically in relative comparisons. For functional integration (Geff), absolute comparisons enhanced values compared with relative comparisons during hot, and hot stimulation increased Geff compared to warm stimulation exclusively in absolute comparisons. Small-worldness was elevated in absolute comparisons for both stimuli, with warm stimulation increasing Sw across methods. Modularity (Mod) was higher in absolute comparisons, with hot stimulation enhancing Mod in both methods. Detailed statistical results are in Supplementary Table 3, http://links.lww.com/PAIN/C435.

In summary, the graph analysis revealed that absolute comparisons exhibited higher functional segregation (Gcc), greater small-world properties (Sw), and enhanced information processing capabilities (Mod) compared to relative comparisons across both stimulus conditions in the source space. These results aligned with sensor-space findings, which also indicated reduced segregation for hot stimuli in relative comparisons and enhanced integration for hot stimuli in absolute comparisons.

3.4. Higher-order intranetwork and internetwork connectivity strength results

To understand better the brain-wide graph connectivity dynamics, we categorised them into intranetwork and internetwork connections. Intranetwork connectivity (Fig. S2, http://links.lww.com/PAIN/C435, top) showed increased hot-stimulation connectivity in SomMot, Limbic, and Cont networks for absolute comparisons, and in Cont and SomMot (marginally) for relative comparisons. Conversely, relative comparisons exhibited increased warm-stimulation connectivity in Visual, DorsAttn, SalVentAttn, and Default networks. For internetwork connectivity (Fig. S2, http://links.lww.com/PAIN/C435, bottom), absolute comparisons demonstrated higher hot-stimulation connectivity in Limbic and Cont networks, with no significant effects in relative comparisons. Detailed statistical results are in Supplementary Table 4, http://links.lww.com/PAIN/C435.

In summary, Limbic and Cont networks exhibited significantly higher intranetwork connectivity associated with hot stimulation in both comparisons. Moreover, SomMot network also showed significantly higher intranetwork connectivity in absolute comparison but marginally higher intranetwork connectivity for relative comparison.

3.5. Higher-order intra-somato-motor graph results

3.5.1. Intra-somato-motor connectivity results

Focussing on the SomMot network (**Fig. 4**), group-level graphs exhibited distinct bilateral patterns with a concentration of connections in the right hemisphere in both comparison methods and stimulus conditions (**Fig. 4A**). Although no significant graphs were found post-NBS, *t*-graphs illustrated connections with *t*-values greater than zero. The hot contrast exhibited a bilateral pattern in the absolute comparison (**Fig. 4A** second row first column), whereas in the relative comparison, it showed a left hemisphere-dominated pattern accompanied by cross-hemispheric connections (**Fig. 4A** second row third column). In contrast, the warm contrast (**Fig. 4A** second row second and fourth columns) exhibited a right hemisphere-dominant pattern across both comparison methods.

In summary, we observed that during tonic pain, although not surviving statistical correction, the SomMot network shifted from a right hemisphere-dominant, clustered organisation (warm condition) to a more bilateral, distributed connectivity profile (hot condition) in both comparison methods (**Fig. 4A**, second row).

3.5.2. Intra-somato-motor graph results

In the analysis of SomMot graph inferences, only functional segregation (Gcc) showed significant effects (**Fig. 4B**). The absolute comparison produced higher Gcc than relative for both stimulus conditions, whereas warm stimulation consistently enhanced Gcc versus hot stimulation across both comparison methods. This pattern aligns with the observed right hemisphere-dominated clustering in warm condition graphs compared to the less clustered intra-SomMot connectivity in hot condition graphs (detailed statistical results are in Supplementary Table 5, http://links.lww.com/PAIN/C435).

In summary, for connections within the SomMot network across both stimulus conditions, the absolute comparison demonstrated greater functional segregation (Gcc) than relative comparison. Moreover, across both comparison methods, distinct processing dynamics were reflected in significant differences in global segregation, which may account for the contrasting connectivity patterns between conditions. Specifically, Gcc associated with warm stimulation was significantly larger than that induced by hot stimulation, likely because of the distribution of less clustered edges within intra-SomMot connectivity in the hot condition's *t*-graphs (**Fig. 4** second row first and third columns). In contrast, right hemisphere-dominated patterns with greater clustering were observed in the warm condition's *t*-graphs (**Fig. 4** second row second and fourth columns).

3.6. Higher-order internetwork graph results

3.6.1. Internetwork connectivity results

For the internetwork graph results (**Fig. 5**), although no statistically significant effects were observed, both comparison

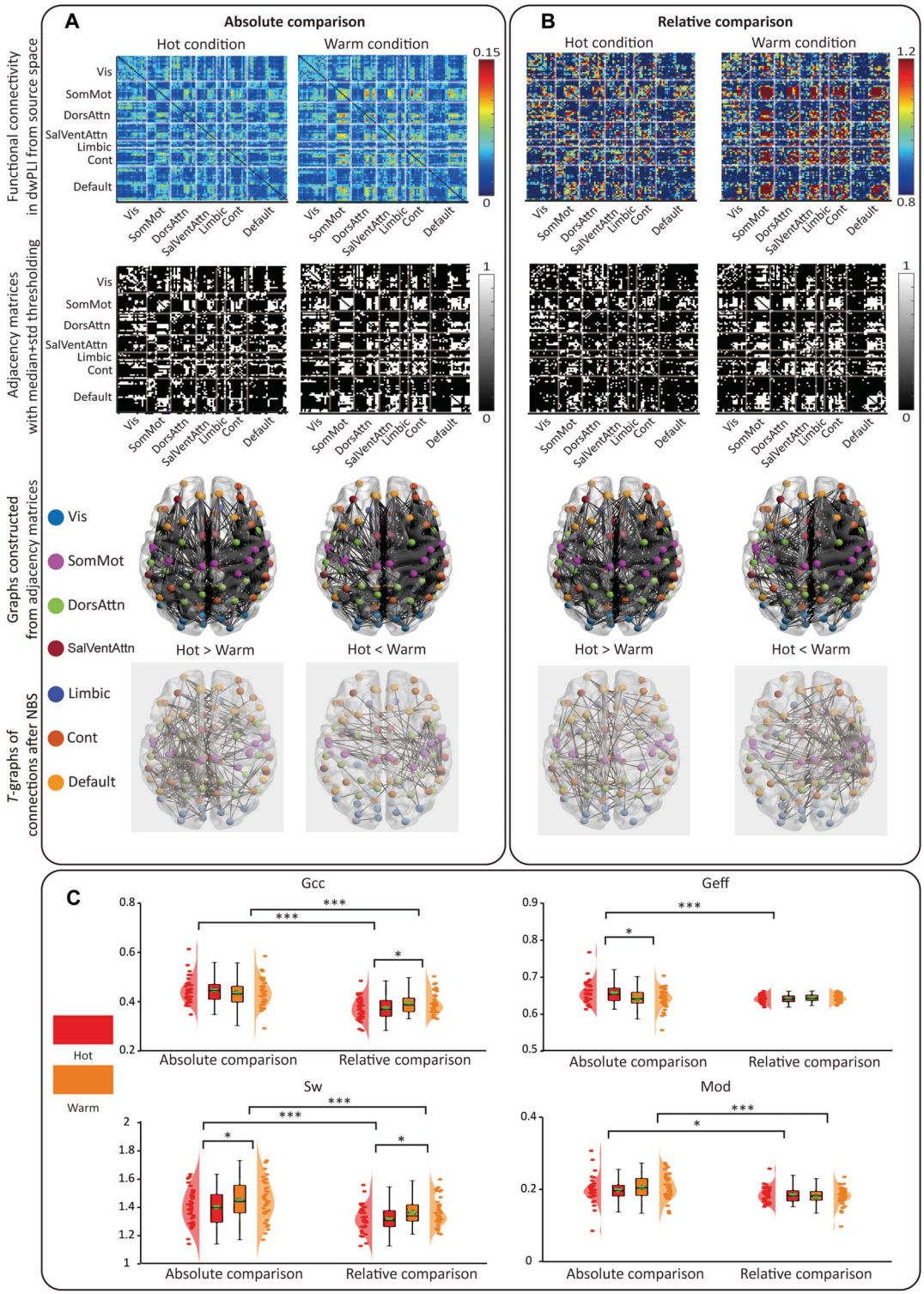

Figure 3. Functional graphs elicited by hot and warm stimulation using 2 comparison methods in source space. (A) Group-level functional connectivity matrices for hot and warm stimulation (first row) projected in source space for 100 pairs of brain regions organised into 7 different functional networks (Visual, Somato-motor, Dorsal Attention, Salience-Ventral Attention, Limbic, Control, and Default). Adjacency matrices (second row) were constructed as absolute, unweighted graphs (third row), *t*-graphs (fourth row) constructed from connections with a *t*-value larger than 1.7 compared between conditions using NBS (shown in reduced opacity indicate nonsignificant results). The left panel showed hot-preferred responses, and the right panel showed warm-preferred responses. (B) Similar to (A) but using a relative comparison. (C) Violin plots with overlaid scatter, and box plots illustrate the results of repeated-measures ANOVA with Bonferroni correction for post hoc comparisons of 4 GNIs across the hot (red) and warm (orange) conditions and 2 comparison methods. A green-filled circle with a black edge denotes the mean value for each group. A stable pattern emerged across both comparison methods, with the hot condition showing a bilateral distribution of connectivity, whereas the warm condition exhibited a right-lateralised distribution. Notably, hot stimulation consistently elicited increased connectivity in the left frontoparietal regions, whereas the warm condition was associated with enhanced connectivity around the SomMot network. Graphs evoked by the hot stimulus exhibited a significantly lower degree of functional segregation in the relative comparison and a significantly higher degree of functional integration in the absolute comparison compared to those from warm stimulation, which were consistent with the results in sensor space. $^{*}P < 0.05$, $^{***}P < 0.001$. Gcc, global clustering coefficient; Geff, global efficiency; GNIs, global network inferences; Mod, modularity; NBS, network-based statistics; SomMot, somato-motor; Sw, small-worldness.

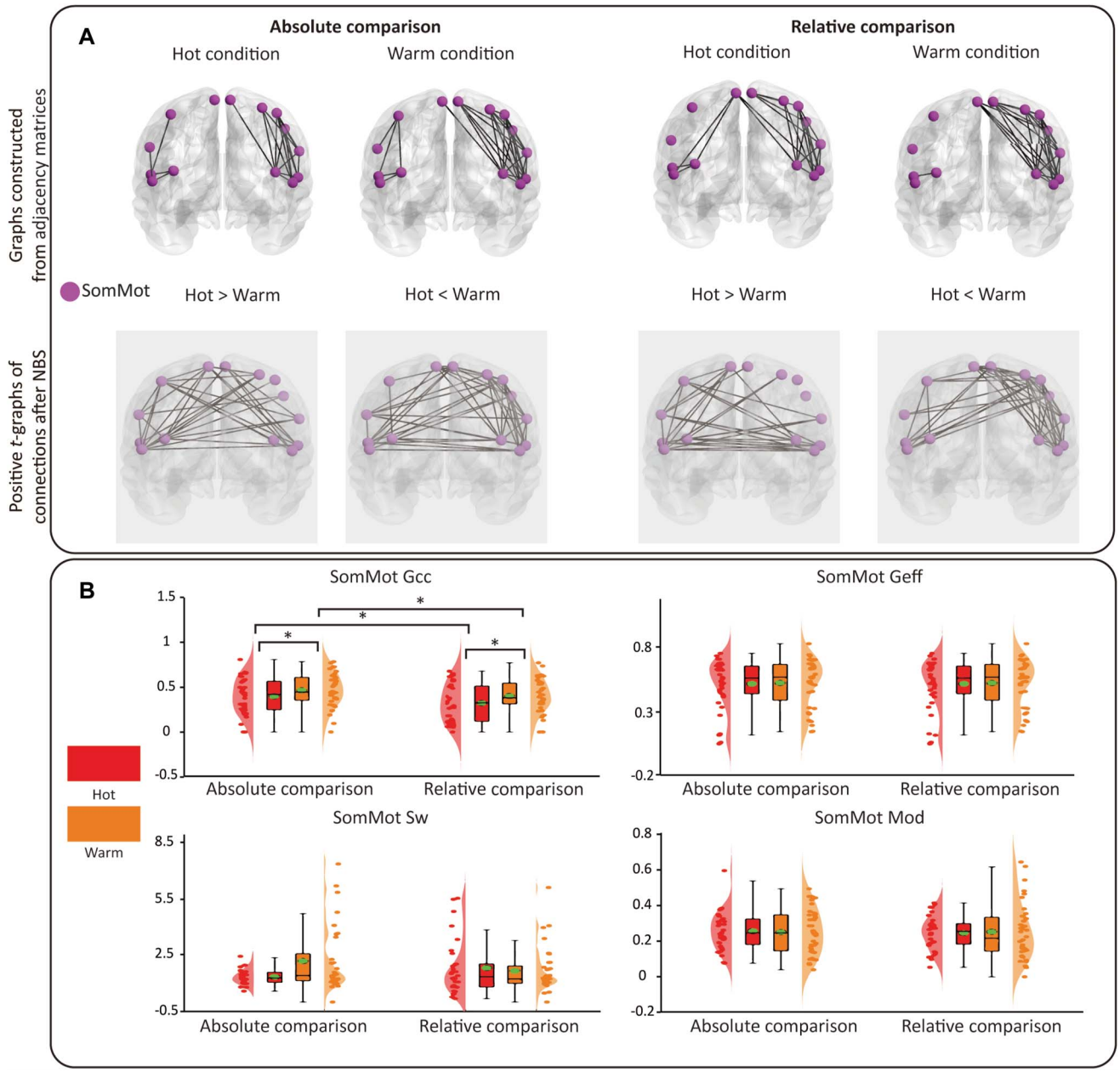

Figure 4. Higher-order intra-SomMot graph. (A) Group-level intranetwork graphs (upper panel) for the SomMot and corresponding *t*-graphs ($t > 0$; reduced opacity indicate nonsignificant results, in the lower panel) were generated after NBS analysis across different stimulus conditions. The left-half panel for absolute comparison and the right-half panel for relative comparison. (B) Violin plots with overlaid scatter, and box plots illustrate the results of repeated-measures ANOVA with Bonferroni correction for post hoc comparisons of 4 GNIs across the hot (red) and warm (orange) conditions and 2 comparison methods. A green-filled circle with a black edge denotes the mean value for each group. The *t*-graphs from both comparison methods showed less clustered edges distributed bilaterally within intra-SomMot connectivity in hot-preferred comparisons and a right hemisphere-dominated pattern with greater clustering in the warm-preferred comparisons. The Gcc induced by warm stimulation was significantly larger than that induced by hot stimulation in both comparison methods. $^{*}P < 0.05$, $^{***}P < 0.001$. Gcc, global clustering coefficient; Geff, global efficiency; GNIs, global network inferences; Mod, modularity; NBS, network-based statistics; SomMot, somato-motor; Sw, small-worldness.

methods consistently indicated greater internetwork communication during hot stimulation compared to warm stimulation. Moreover, the *t*-graphs for the hot contrast in both comparison methods highlighted increased involvement of the DorsAttn and SomMot networks (**Fig. 5A**, third row, first and third columns).

3.6.2. Internetwork graph results

Local graph inferences were computed using Ebc and Lcc for each network in the weighted graph (**Fig. 5B**). Although the effects did not survive statistical correction, the *t*-graph after NBS revealed distinct edges centred on the SomMot network for the hot contrast under the absolute comparison (**Fig. 5B**, upper panel, first column). For Ebc in the hot contrast under the relative comparison, the *t*-graph shared 4 edges with that of the absolute comparison. Among these, 2 edges (SomMot-Limbic and SomMot-Cont) represented connections linking the SomMot network with other networks (**Fig. 5B**, upper panel, third column).

All 7 networks exhibited significantly higher Lcc under hot versus warm condition in absolute comparison (**Fig. 5B** lower and

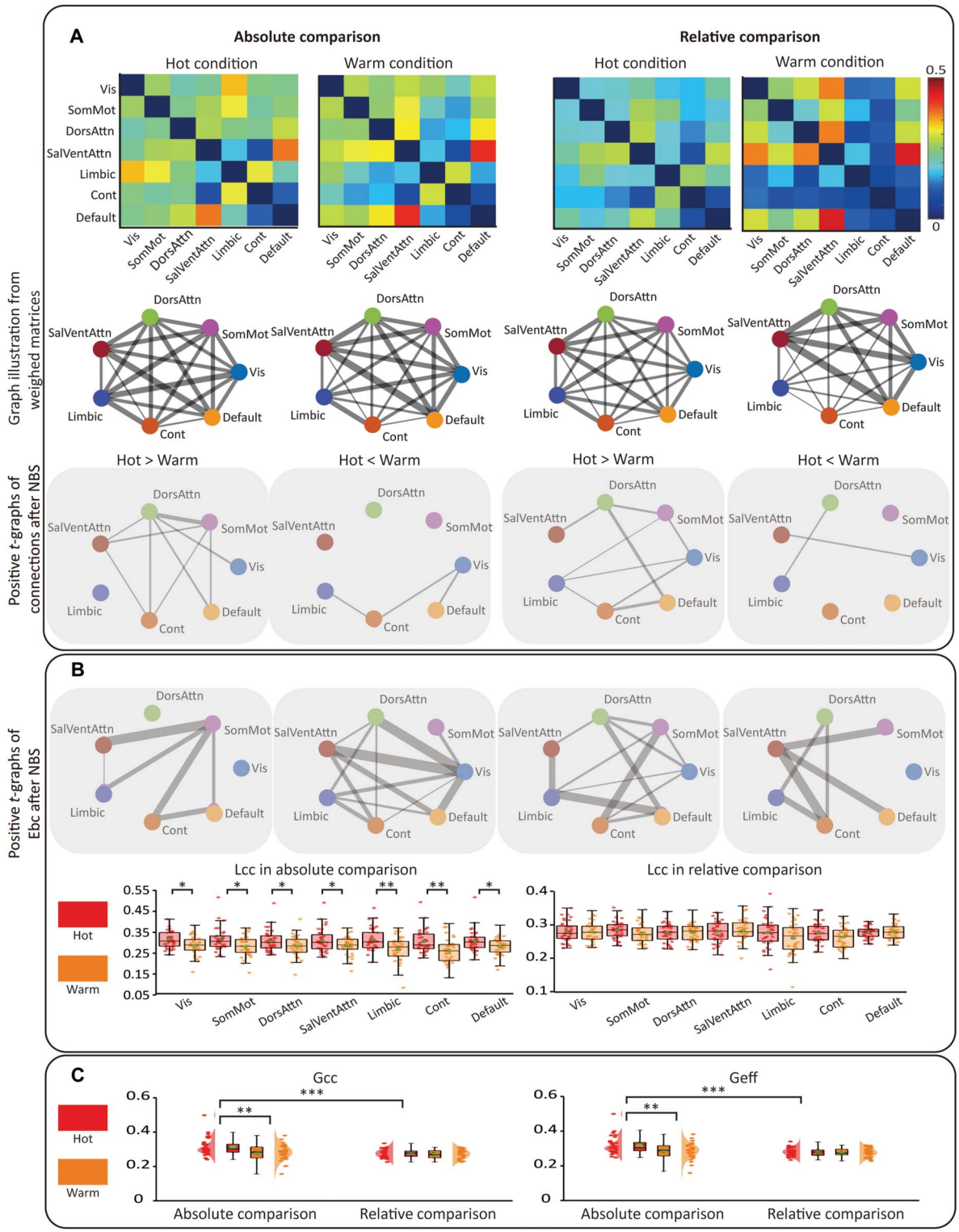

Figure 5. Internetwork analysis and local and global graph inferences for internetwork graph. (A) Group-level internetwork weighted matrices (first and second row) and corresponding *t*-graphs ($t > 0$; reduced opacity indicate nonsignificant results, third row) were generated after NBS analysis across different stimulus conditions. The left-half panel for absolute comparison and the right-half panel for relative comparison. (B) Results for local graph inferences analysis. Ebc corresponded *t*-graphs generated after NBS ($t > 0$; shown in reduced opacity, upper panel); box plots illustrate the statistical analysis for Lcc by paired-sample *t* test with FDR correction between stimulus conditions for 2 comparison methods (lower panel). (C) Violin plots with overlaid scatter and box plots show the results of repeated-measures ANOVA with Bonferroni correction for post hoc comparisons of 2 GNIs across the hot (red) and warm (orange) conditions and 2 comparison methods. A green-filled circle with a black edge denotes the mean value for each group. The *t*-graphs illustrating both higher internetwork connectivity and Ebc evoked by hot stimulation emphasised the importance of edges connecting the SomMot network with other networks in both comparison methods. In absolute comparison, higher Lcc across all networks leading to significant higher Gcc in hot condition for internetwork graph. $^{*}P < 0.05$, $^{***}P < 0.001$. Ebc, edge betweenness centrality; Gcc, global clustering coefficient; Geff, global efficiency; GNIs, global network inferences; Lcc, local clustering coefficient; NBS, network-based statistics; SomMot, somato-motor.

left panel), whereas relative comparison (**Fig. 5B** lower and right panel) showed no significant differences (detailed statistics are in Supplementary Table 6, http://links.lww.com/PAIN/C435).

For GNIs from internetwork connections (**Fig. 5C**), both functional segregation (Gcc) and integration (Geff) showed significant stimulus and comparison method effects. Absolute comparison revealed higher Gcc and Geff for hot versus warm stimulation, whereas relative comparison enhanced both metrics exclusively under hot stimulation. This divergence from intranetwork findings reflects hot stimulation's stronger internetwork connectivity, evidenced by greater edge density and edge betweenness centrality in *t*-graphs. Crucially, these patterns highlight SomMot network's crosstalk with other networks, particularly through connections strengthened by hot stimulation (detailed statistics are in Supplementary Table 5, http://links.lww.com/PAIN/C435).

In summary, the GNIs indicated that absolute comparison demonstrates greater functional segregation (Gcc) for internetwork connections recruited by hot stimulation (**Fig. 5C**). The significantly greater Gcc in the internetwork connectivity matrix in the hot compared to the warm condition may be attributed to the significantly higher Lcc in each network from that graph (**Fig. 5B** lower and left panel), reflecting overall enhanced network communication during noxious stimulation. Although NBS-based condition-contrast *t*-graphs did not survive statistical correction, their spatial patterns showed alignment with the network inferences results. Specifically, the larger number of edges in *t*-graph, which represents larger internetwork connectivity evoked by hot than warm stimulation in absolute comparison (**Fig. 5A** third row, left-half panel), was consistent with the significant segregation effects captured by Gcc and Lcc.

These patterns were particularly evident in connections involving the SomMot. The *t*-graphs illustrating both higher internetwork connectivity (**Fig. 5A** third row first and third columns) and Ebc evoked by hot stimulation (**Fig. 5B** upper panel first and third columns) emphasised the importance of edges connecting the SomMot network with other networks in both comparison methods. Therefore, the higher-order internetwork graphs highlight the crosstalk of SomMot with other networks.

Although these edge-level patterns should be interpreted cautiously given their nonsignificant status, they provide complementary spatial context to the significant network-level findings revealed by graph-theoretical analysis.

3.7. Correlation between global network inferences and self-report data

We assessed condition-specific relationships between GNIs and unpleasantness ratings for both absolute and relative comparisons (**Table 1**). Under absolute comparisons, 6 significant associations were identified (**Fig. 6A**): For the warm condition, sensor space Geff showed a positive correlation ($r = 0.38$, $P_{(uncorrected)} = 0.02$), whereas source space Geff exhibited a negative correlation ($r = -0.40$, $P_{(uncorrected)} = 0.02$) with unpleasantness. Moreover, internetwork Gcc and Geff positively correlated with unpleasantness during the hot condition (Gcc: $r = 0.35$, $P_{(uncorrected)} = 0.04$; Geff: $r = 0.34$, $P_{(uncorrected)} = 0.04$), whereas the same GNIs inversely correlated with unpleasantness during the warm condition (Gcc: $r = -0.40$, $P_{(uncorrected)} = 0.02$; Geff: $r = -0.38$, $P_{(uncorrected)} = 0.02$). These findings suggest that internetwork Gcc and Geff differentially encode tonic hot and warm perception, with opposing directional effects between the 2 conditions. In contrast, relative comparisons revealed no significant correlations between individual GNIs and unpleasantness ratings (all $P > 0.05$).

No significant correlations were observed between participant age and any GNIs. Similarly, after controlling for age and sex using partial correlation, no significant relationships were found between GNIs and individual differences in pain perception (defined as the mean unpleasantness difference between hot and warm conditions) or pain tolerance (operationalised as the change in unpleasantness from the first to last third of hot stimulation) (all $P > 0.05$).

However, significant associations emerged between GNIs and pain-related psychological traits. Pain catastrophising, as measured by the PCS, showed significant positive correlations with 3 GNIs derived from the hot condition in the absolute comparison: source space Gcc ($r = 0.55$, $P_{(uncorrected)} = 0.01$); Gcc and Geff from internetwork graph (both $r = 0.44$, $P_{(uncorrected)} = 0.04$). Conversely, trait anxiety (STAI-T) was negatively correlated with 6 GNIs under the warm condition: Gcc in absolute condition from intra-SomMot graph ($r = -0.44$, $P_{(uncorrected)} = 0.04$), Gcc and Geff in relative comparison from source space graph (Gcc: $r = -0.53$, $P_{(uncorrected)} = 0.01$; Geff: $r = -0.50$, $P_{(uncorrected)} = 0.02$), Gcc in relative comparison from intra-SomMot graph ($r = -0.48$, $P_{(uncorrected)} = 0.02$), and Gcc and Geff in relative comparison from internetwork graph (both $r = -0.50$, $P_{(uncorrected)} = 0.02$).

In sum, pain catastrophising was associated with greater segregation and integration during noxious stimulation, whereas higher trait anxiety was associated with reduced network segregation and integration during innocuous warmth. Together, these findings suggest that pain-related psychological traits (pain catastrophising and anxiety) may affect functional network characteristics during noxious and innocuous thermal stimulation, even in the absence of effects related to age and sex. Yet, due to the explorative nature of these correlation, and the absence of a multiple comparison correction of the alpha value, these relationships should be further tested before drawing any confident conclusion.

3.8. Classification performance using global network inferences

The SVM classifier robustly distinguished tonic hot and warm conditions using GNIs derived from combined graph inferences, with the top 3 models based on absolute comparison and showed in **Figure 6B**. The highest-performing model, integrating GNIs from sensor space, source space, and internetwork graphs, achieved an AUC-ROC of 0.94 ($P < 0.001$), with an accuracy of 86%, sensitivity of 0.78, and specificity of 0.92. The second-ranked model attained an accuracy of 85%, sensitivity of 0.75, and specificity of 0.89 (AUC-ROC = 0.93, $P < 0.001$) from GNIs in sensor space and internetwork graphs. Combining GNIs from sensor and source space graphs results in the third best performance, with an accuracy of 83%, sensitivity of 0.78, and specificity of 0.89 (AUC-ROC = 0.92, $P < 0.001$). These results demonstrate the robust discriminative power of GNIs, particularly when combining multimodal graph features, in distinguishing between tonic hot and warm states. The high performance (accuracy above 80% and AUC-ROC above 0.90) highlights their potential as a biomarker framework for decoding tonic pain-related neurophysiological mechanisms.

4. Discussion

We systematically examined EEG functional connectivity patterns during tonic thermal pain in healthy volunteers using network-

based statistics and graph theory-based analysis. Our study yielded 4 main findings. First, we identified a significant brain-wide reorganisation of connectivity during tonic pain, marked by a shift from functional segregation to integration. Second, segregation effects confirmed the transition from intra- to internetwork communication with enhanced SomMot-centred crosstalk. Third, machine learning models successfully distinguished hot from warm states using GNIs (highest AUC-ROC of 0.94; accuracy of 86%; **Fig. 6B**), demonstrating robust discriminative power. Fourth, we highlight the critical influence of comparison methods and thresholding strategies.

4.1. Reorganisation of the brain-wide graph from segregation to integration

We observed a consistent and significant decline in functional segregation (specialisation) and enhanced functional integration (efficiency of global information flow) during tonic pain in both sensor and source spaces (**Figs. 2C and 3C**). This shift, accompanied by significantly decreased modularity (Mod, **Fig. 2C**) and small-worldness (Sw, **Fig. 3C**), suggested a shift toward a more randomised and less cost-efficient network architecture.[36] These findings aligned with alternations observed in the neuropathic pain patients,[65] and a multicentre study in chronic pain cohorts,[39] indicating a fundamental and sustained characteristic shared between experimental tonic pain and clinical chronic pain, which may reflect robust nociceptive integration.[19,69]

This global topological alteration was underpinned by a reorganisation of brain-wide connectivity. In sensor space, we identified significantly different connectivity patterns (**Figs. 2A and B**). Although these patterns did not survive statistical correction in source space, the consistent trend supports the reliability of the topological reorganisation: a shift from contralateral functional specialised sensorimotor connectivity during warm (**Figs. 3A and B**, fourth row right panel; **Fig. 4A**, lower panel second and fourth columns) to ipsilateral integrated frontoparietal connectivity during pain (**Figs. 3A and B**, fourth row left panel). The emergent frontoparietal pattern, associated with the cognitive control network,[26,29] is implicated in attention, salience processing, and top-down modulation of pain.[7,59] Conversely, innocuous warmth was associated with strengthened contralateral sensorimotor connectivity (**Figs. 3A and B**, fourth row right panel; **Fig. 4A**, lower panel second and fourth column). The absence of the contralateral connectivity during pain might be linked to local suppressions of alpha-band oscillations originating in the sensorimotor cortex.[43,44,47,50,63] This asymmetry may reflect alpha-band event-related desynchronisation, which through thalamocortical circuits[16,25] and gamma-aminobutyric acid inhibition,[20,37] may indicate selective gating of information flow, suppression of irrelevant sensory input, and engagement of top-down cognitive processes for attention.[18,25,48]

4.2. Transition of the somato-motor network

The innocuous warmth exhibited significant higher Gcc in the SomMot network (**Fig. 4B**), reflecting higher functional specialisation. This finding aligns with prior identification of a distinct processing system overlapping with resting-state modules and subserving sensory-discriminative functions,[69] whereas the noxious hot pattern aligns with SomMot integration with control and ventral attention (salience) networks.[21,31,32,69]

This network property difference was reflected in the connectivity pattern within SomMot, with the warm condition producing a right hemisphere-dominated pattern (**Fig. 4A**, lower panel second and fourth columns), in contrast with a more bilateral distribution for the hot condition (**Fig. 4A**, lower panel first and

Table 1

Correlation coefficients between global network inferences and unpleasantness ratings across graph types and comparison methods during hot and warm conditions.

Conditions	Type of graphs	Comparison method	Correlation coefficient ($P_{[uncorrected]}$)			
			Gcc	Geff	Sw	Mod
Hot	Sensor space	Absolute	0.09 (0.60)	−0.11 (0.51)	0.04 (0.81)	0.17 (0.33)
		Relative	0.04 (0.80)	0.00 (0.99)	0.05 (0.78)	0.28 (0.10)
	Source space	Absolute	0.20 (0.25)	0.29 (0.09)	−0.12 (0.50)	−0.24 (0.17)
		Relative	−0.12 (0.47)	0.12 (0.48)	−0.21 (0.23)	−0.10 (0.57)
	Intra-SomMot	Absolute	−0.01 (0.93)	0.23 (0.19)	—	0.05 (0.77)
		Relative	0.22 (0.20)	0.14 (0.42)	—	0.04 (0.82)
	Internetwork	Absolute	**0.35 (0.04)**	**0.34 (0.04)**	—	—
		Relative	0.17 (0.32)	0.16 (0.35)	—	—
Warm	Sensor space	Absolute	0.18 (0.30)	**0.38 (0.02)**	0.04 (0.84)	0.21 (0.21)
		Relative	0.22 (0.19)	−0.14 (0.43)	0.25 (0.14)	−0.26 (0.13)
	Source space	Absolute	−0.29 (0.09)	**−0.40 (0.02)**	0.06 (0.74)	0.04 (0.82)
		Relative	0.06 (0.75)	0.07 (0.68)	0.10 (0.57)	−0.05 (0.79)
	Intra-SomMot	Absolute	−0.07 (0.66)	−0.11 (0.51)	—	−0.10 (0.55)
		Relative	0.11 (0.51)	0.04 (0.80)	—	−0.11 (0.51)
	Internetwork	Absolute	**−0.40 (0.02)**	**−0.39 (0.02)**	—	—
		Relative	−0.05 (0.78)	−0.03 (0.89)	—	—

Correlations were computed between GNIs and mean participant-level unpleasantness ratings. Statistically significant results ($P < 0.05$) are highlighted in bold. All correlations are reported using uncorrected P values.
Gcc, global clustering coefficients; Geff, global efficiency; GNIs, global network inferences; Mod, modularity; SomMot, somato-motor; Sw, small-worldness.

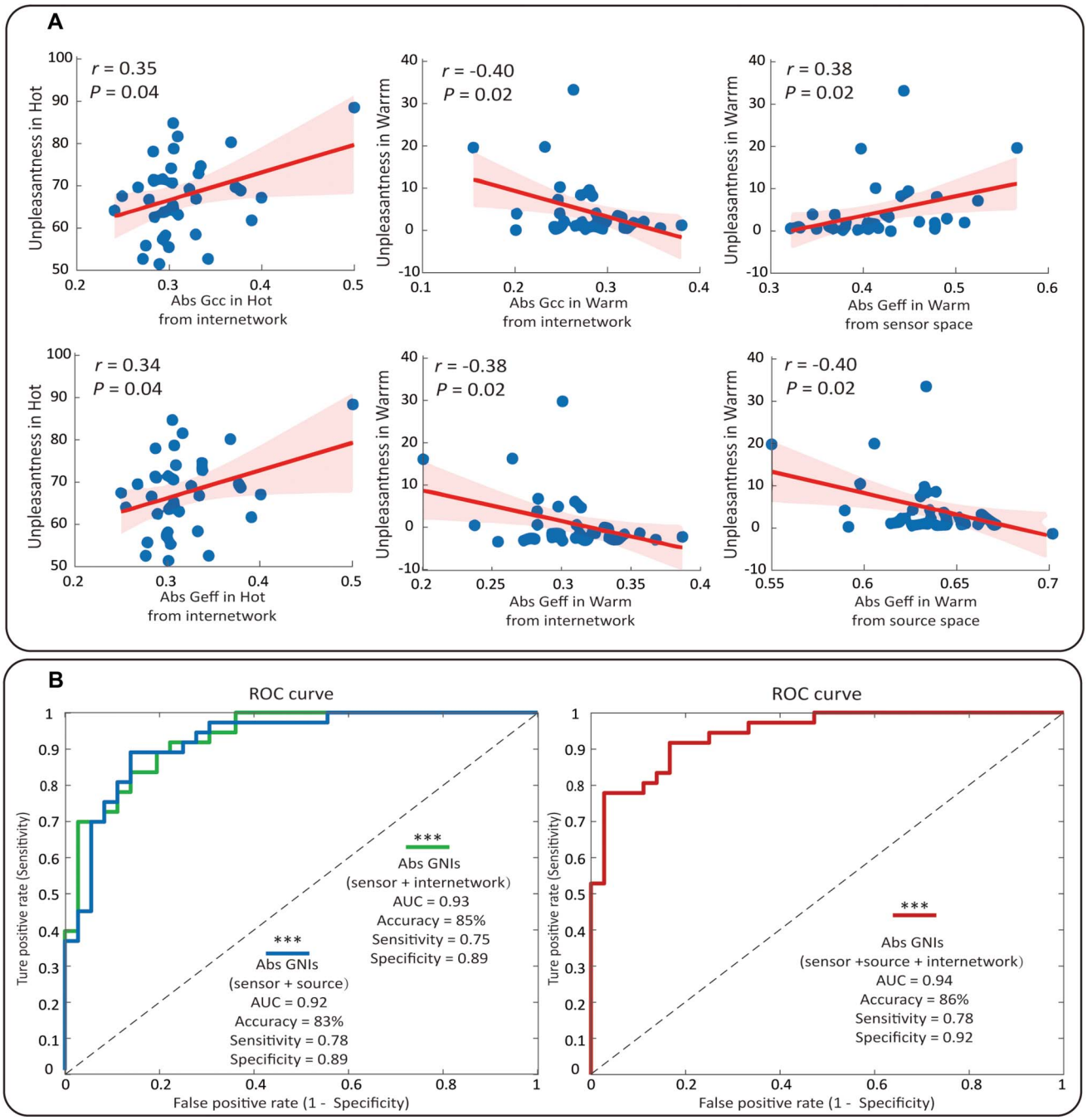

Figure 6. Correlation between single GNIs and behavioural ratings, and classification performance. (A) Scatter plots with linear fit and 95% confidence intervals illustrating the correlations between significant individual GNIs and unpleasantness ratings within each stimulation condition. All correlations are reported using uncorrected *P*-values and should be interpreted with caution. (B) Classification performance was evaluated using leave-one-subject-out cross-validation with an SVM classifier. The top 3 performing models are presented, with the best performance highlighted in red, the second-best in green, and the third in blue. The highest classification performance was achieved using a combination of GNIs derived from sensor space, source space, and internetwork graphs, yielding an AUC-ROC of 0.94, an accuracy of 86%, a sensitivity of 0.78, and a specificity of 0.92. ***$P < 0.001$. Abs, absolute comparison; AUC, area under curve; Gcc, global clustering coefficients; Geff, global efficiency; GNIs, global network inferences; ROC, receiver operating characteristic; SVM, support vector machine.

third columns). Although these connectivity patterns were not statistically significant, their alignment across comparison methods supports a dynamic shift in SomMot processing.

Furthermore, we found consistent, although nonsignificant, greater number of edges clustering around the SomMot (**Fig. 5A**, third row first and third columns) as well as greater Ebc (**Fig. 5B**, upper panel first and third columns), highlighting the SomMot central role in between-network communication. This adaptability may reflect rapidly increased synaptic plasticity in the primary somatosensory cortex induced by nociception,[5,23,28] mechanisms potentially disrupted in chronic pain.[24,49,62] Taken together, these findings highlight the SomMot network's dual functionality: localised sensory processing for nonpainful somatosensory experience versus integrative coordination during pain.

4.3. Shift from intranetwork to internetwork connectivity

We observed decreased segregation at the brain-wide level during tonic pain (lower Gcc; **Figs. 2C and 3C**) whereas internetwork connectivity exhibited increased local clustering (Lcc; **Fig. 5B**) and segregation (higher Gcc; **Fig. 5C**). This discrepancy arose from the exclusion of intranetwork connections, which artificially inflated Gcc by removing interconnected local clusters. This methodological distinction explains conflicting prior results: although the community detection method found increased Gcc with reduced connectivity between an integrated "pain supersystem" and other networks during pain,[69] canonical network analysis using atlas defined parcellation (like ours) reported increased segregation (Gcc) only during the innocuous condition, with enhanced between-network connectivity.[19]

Based on Gcc variations, intranetwork connections prioritise nociceptive information, facilitating a shift from segregated to integrated brain states. This was observed in the SomMot network and aligns with reduced intranetwork connectivity found in sustained myofascial pain[21] and patients with fibromyalgia,[22] indicating a transition from functional specialisation under innocuous stimulation to broader integration during pain experience.

Such integration was also reflected by overall elevation of Lcc (**Fig. 5B**, lower panel absolute comparison) and greater number of edges in the internetwork graphs (**Fig. 5A**, third row first and third columns). These results align with previous research showing that thermal pain induces a brain-wide shift from segregation to integration, with enhanced between-network connectivity.[19] Specifically, capsaicin-induced sustained pain has been associated with the emergence of a SomMot-dominant neural community, wherein ventral primary SomMot regions showed dissociated from their original network and incorporated with subcortical and frontoparietal regions.[32] A finding also replicated in patients with chronic low back pain[70] and postherpetic neuralgia.[34]

In summary, although methodological factors explain Gcc discrepancies, our results converge to show that tonic pain induces an alteration from localised functional specialisation within intranetwork to enhanced internetwork communication and global integration. This reorganisation, centred on SomMot connectivity, underscores the dynamic balance between segregation and integration in shaping pain-related brain states.[14,27]

4.4. Global network inferences as a potential translational biomarker

GNIs achieved high classification performance in distinguishing noxious hot from innocuous warm stimulation and identified significant links with pain-related psychological states. Psychological traits modulated pain-related network reorganisation in distinct and clinically relevant ways: catastrophising predominantly influenced responses to noxious stimuli, whereas anxiety affected innocuous sensory processing.

Although our findings provide a general model of pain-related network dynamics under controlled conditions, their generalisation to chronic pain populations warrants caution. Chronic pain involves neuroplastic adaptations and compensatory mechanisms that may alter functional network signatures, with psychological influences potentially amplified.

Translating GNIs into clinically useful biomarkers will require validation in large, multicentre datasets accounting for comorbidities, medication, and pain duration. Future work should also explore the use of GNIs for real-time monitoring of psychological states and their integration into closed-loop neuromodulation, ensuring interpretability and reliability across clinical contexts.

4.5. Methodological considerations: comparison methods and thresholding strategies

Our analysis revealed consistent connectivity patterns and network inferences across both comparison methods. This demonstrates the robustness of the identified condition-contrast effects and underscores the complementary value of using both approaches, which together provide a more comprehensive characterisation of brain network reorganisation.

Our decision to retain weak connections in thresholding strategies may resolve conflicting reports on GNIs such as Gcc.[35,39,44,69] Arbitrary thresholding criteria, such as retaining only the top 10% of strongest connections or iterating across densities (eg, 10%-30%) and then averaging Gcc values across these arbitrary cutoffs, risk conflating reorganisation of strong, hub-dominated connections and subtler reconfigurations in weak but topologically critical edges. By contrast, including weaker connections captures nuanced shifts in network topology. This aligns with prior evidence that thresholding strategies critically influence neuroimaging outcome,[2] and that weak connections, often dismissed as noise, may underpin cognitive flexibility and network resilience.[54]

4.6. Limitations

The main caveat of the current study is that our conclusions are primarily drawn from *t*-graphs, except from the significant *P*-graphs derived from sensor space. The absence of statistically significant connectivity graphs limits the robustness of our interpretation. This issue should be addressed in future research with larger sample sizes and multiple datasets to increase statistical power and improve the detection of reproducible network alterations after multiple comparisons correction. In addition, although our classifier achieved high performance (AUC-ROC $>$ 0.9), its generalisability and validity need to be further evaluated using independent datasets to ensure its applicability in broader contexts.

5. Conclusion

Altogether, these findings provide compelling evidence that tonic experimental pain in healthy volunteers is associated with significant reorganisation of alpha EEG connectivity. The hallmark of this reorganisation is a shift from high intranetwork functional segregation (especially the SomMot network) to internetwork integration via enhanced communication. Furthermore, the robust predictive performance of GNIs highlights their translational potential as biomarkers for pain states. Our approach also demonstrates the importance of including both strong and weak connections as well as baseline assessment. Such methodological approach not only reconciles conflicting reports in the literature but also sets a foundation for future studies aimed at elucidating the neural substrates of chronic pain and its clinical translation.

Conflict of interest statement

The authors have no conflicts of interest to declare and used generative AI to assist with narrative improvement.

Acknowledgments

The authors thank Daisy McInnerney, Jason Cooke, and Istvan L. Gyimes for helping with the preparation and data collection of the original experiment. The authors thank Sebastian Halder for providing feedback on the correctness of the machine learning approach to feature selection. The refrigerated and heating bath was purchased by means of a Departmental Research Promotion and impact Fund award to E.V. The authors acknowledge the use of the High-Performance Computing Cluster (CERES) and support services at the University of Essex. The software scripts and data files used for the analyses are available on a dedicated OSF repository (https://osf.io/wdxra/).

References

[1] Achard S, Bullmore E. Efficiency and cost of economical brain functional networks. PLoS Comput Biol 2007;3:e17.
[2] Adamovich T, Zakharov I, Tabueva A, Malykh S. The thresholding problem and variability in the EEG graph network parameters. Sci Rep 2022;12:18659.
[3] Alain C, Arnott SR, Hevenor S, Graham S, Grady CL. "What" and "where" in the human auditory system. Proc Natl Acad Sci 2001;98:12301–6.
[4] Barabasi DL, Bianconi G, Bullmore E, Burgess M, Chung S, Eliassi-Rad T, George D, Kovacs IA, Makse H, Nichols TE, Papadimitriou C, Sporns O, Stachenfeld K, Toroczkai Z, Towlson EK, Zador AM, Zeng H, Barabasi AL, Bernard A, Buzsaki G. Neuroscience needs network science. J Neurosci 2023;43:5989–95.
[5] Cao F-L, Xu M, Gong K, Wang Y, Wang R, Chen X, Chen J. Imbalance between excitatory and inhibitory synaptic transmission in the primary somatosensory cortex caused by persistent nociception in rats. J Pain 2019;20:917–31.
[6] Cohen MX. Analyzing neural time series data: theory and practice. Cambridge, MA: MIT Press; 2014.
[7] Corbetta M, Shulman GL. Control of goal-directed and stimulus-driven attention in the brain. Nat Rev Neurosci 2002;3:201–15.
[8] Delorme A, Makeig S. EEGLAB: an open source toolbox for analysis of single-trial EEG dynamics including independent component analysis. J Neurosci Methods 2004;134:9–21.
[9] Eldabe S, Obara I, Panwar C, Caraway D. Biomarkers for chronic pain: significance and summary of recent advances. Pain Res Manag 2022; 2022:1–6.
[10] Feng L, Li H, Cui H, Xie X, Xu S, Hu Y. Low back pain assessment based on alpha oscillation changes in spontaneous electroencephalogram (EEG). Neural Plast 2021;2021:1–11.
[11] Gil Ávila C, Bott FS, Tiemann L, Hohn VD, May ES, Nickel MM, Zebhauser PT, Gross J, Ploner M. DISCOVER-EEG: an open, fully automated EEG pipeline for biomarker discovery in clinical neuroscience. Sci Data 2023;10:613.
[12] Goldman D. The clinical use of the "average" reference electrode in monopolar recording. Electroencephalogr Clin Neurophysiol 1950;2:209–12.
[13] Granot M, Weissman-Fogel I, Crispel Y, Pud D, Granovsky Y, Sprecher E, Yarnitsky D. Determinants of endogenous analgesia magnitude in a diffuse noxious inhibitory control (DNIC) paradigm: do conditioning stimulus painfulness, gender and personality variables matter? PAIN 2008;136:142–9.
[14] Hemington KS, Wu Q, Kucyi A, Inman RD, Davis KD. Abnormal cross-network functional connectivity in chronic pain and its association with clinical symptoms. Brain Struct Funct 2016;221:4203–19.
[15] Huang S, Wakaizumi K, Wu B, Shen B, Wu B, Fan L, Baliki MN, Zhan G, Apkarian AV, Huang L. Whole-brain functional network disruption in chronic pain with disk herniation. PAIN 2019;160:2829–40.
[16] Hughes SW, Crunelli V. Thalamic mechanisms of EEG alpha rhythms and their pathological implications. Neuroscientist 2005;11:357–72.
[17] Jackman JS, Bell PG, Van Someren K, Gondek MB, Hills FA, Wilson LJ, Cockburn E. Effect of hot water immersion on acute physiological responses following resistance exercise. Front Physiol 2023;14: 1213733.
[18] Jensen O, Mazaheri A. Shaping functional architecture by oscillatory alpha activity: gating by inhibition. Front Hum Neurosci 2010;4:186.
[19] Kastrati G, Thompson WH, Schiffler B, Fransson P, Jensen KB. Brain network segregation and integration during painful thermal stimulation. Cereb Cortex 2022;32:4039–49.
[20] Kim JA, Davis KD. Neural oscillations: understanding a neural code of pain. Neuroscientist 2021;27:544–70.
[21] Kim J, Loggia ML, Edwards RR, Wasan AD, Gollub RL, Napadow V. Sustained deep-tissue pain alters functional brain connectivity. PAIN 2013;154:1343–51.
[22] Kim J, Loggia ML, Cahalan CM, Harris RE, Beissner F, Garcia RG, Kim H, Barbieri R, Wasan AD, Edwards RR, Napadow V. The somatosensory link in fibromyalgia: functional connectivity of the primary somatosensory cortex is altered by sustained pain and is associated with clinical/autonomic dysfunction. Arthritis Rheumatol 2015;67:1395–405.
[23] Kim W, Kim SK, Nabekura J. Functional and structural plasticity in the primary somatosensory cortex associated with chronic pain. J Neurochem 2017;141:499–506.
[24] Kim H, Mawla I, Lee J, Gerber J, Walker K, Kim J, Ortiz A, Chan S-T, Loggia ML, Wasan AD, Edwards RR, Kong J, Kaptchuk TJ, Gollub RL, Rosen BR, Napadow V. Reduced tactile acuity in chronic low back pain is linked with structural neuroplasticity in primary somatosensory cortex and is modulated by acupuncture therapy. Neuroimage 2020;217:116899.
[25] Klimesch W. Alpha-band oscillations, attention, and controlled access to stored information. Trends Cognit Sci 2012;16:606–17.
[26] Kong J, Jensen K, Loiotile R, Cheetham A, Wey HY, Tan Y, Rosen B, Smoller JW, Kaptchuk TJ, Gollub RL. Functional connectivity of the frontoparietal network predicts cognitive modulation of pain. PAIN 2013; 154:459–67.
[27] Kucyi A, Davis KD. The dynamic pain connectome. Trends Neurosci 2015;38:86–95.
[28] Kuner R, Flor H. Structural plasticity and reorganisation in chronic pain. Nat Rev Neurosci 2017;18:20–30.
[29] Kutch JJ, Labus JS, Harris RE, Martucci KT, Farmer MA, Fenske S, Fling C, Ichesco E, Peltier S, Petre B, Guo W, Hou X, Stephens AJ, Mullins C, Clauw DJ, Mackey SC, Apkarian AV, Landis JR, Mayer EA. Resting-state functional connectivity predicts longitudinal pain symptom change in urologic chronic pelvic pain syndrome: a MAPP network study. PAIN 2017;158:1069–82.
[30] Latora V, Marchiori M. Efficient behavior of small-world networks. Phys Rev Lett 2001;87:198701.
[31] Lee JJ, Kim HJ, Ceko M, Park BY, Lee SA, Park H, Roy M, Kim SG, Wager TD, Woo CW. A neuroimaging biomarker for sustained experimental and clinical pain. Nat Med 2021;27:174–82.
[32] Lee JJ, Lee S, Lee DH, Woo CW. Functional brain reconfiguration during sustained pain. Elife 2022;11:e74463.
[33] Lenoir D, Cagnie B, Verhelst H, De Pauw R. Graph measure based connectivity in chronic pain patients: a systematic review. Pain Physician 2021;24:E1037–58.
[34] Li H, Li X, Wang J, Gao F, Wiech K, Hu L, Kong Y. Pain-related reorganization in the primary somatosensory cortex of patients with postherpetic neuralgia. Hum Brain Mapp 2022;43:5167–79.
[35] Li L, Di X, Zhang H, Huang G, Zhang L, Liang Z, Zhang Z. Characterization of whole-brain task-modulated functional connectivity in response to nociceptive pain: a multisensory comparison study. Hum Brain Mapp 2022;43:1061–75.
[36] Liao X, Vasilakos AV, He Y. Small-world human brain networks: perspectives and challenges. Neurosci Biobehav Rev 2017;77:286–300.
[37] Lőrincz ML, Kékesi KA, Juhász G, Crunelli V, Hughes SW. Temporal framing of thalamic relay-mode firing by phasic inhibition during the alpha rhythm. Neuron 2009;63:683–96.
[38] Lou W, Li X, Jin R, Peng W. Time-varying phase synchronization of resting-state functional magnetic resonance imaging reveals a shift toward self-referential processes during sustained pain. PAIN 2024;165:1493–504.
[39] Mano H, Kotecha G, Leibnitz K, Matsubara T, Nakae A, Shenker N, Shibata M, Voon V, Yoshida W, Lee M, Yanagida T, Kawato M, Rosa MJ, Seymour B. Classification and characterisation of brain network changes in chronic back pain: a multicenter study. Wellcome open Res 2018;3:19.
[40] Modares-Haghighi P, Boostani R, Nami M, Sanei S. Quantification of pain severity using EEG-based functional connectivity. Biomed Signal Process Control 2021;69:102840.

[41] Newman ME. Fast algorithm for detecting community structure in networks. Phys Rev E 2004;69:066133.
[42] Newman ME. Modularity and community structure in networks. Proc Natl Acad Sci 2006;103:8577–82.
[43] Nickel MM, May ES, Tiemann L, Schmidt P, Postorino M, Ta Dinh S, Gross J, Ploner M. Brain oscillations differentially encode noxious stimulus intensity and pain intensity. Neuroimage 2017;148:141–7.
[44] Nickel MM, Ta Dinh S, May ES, Tiemann L, Hohn VD, Gross J, Ploner M. Neural oscillations and connectivity characterizing the state of tonic experimental pain in humans. Hum Brain Mapp 2020;41:17–29.
[45] Oostenveld R, Fries P, Maris E, Schoffelen J-M. FieldTrip: open source software for advanced analysis of MEG, EEG, and invasive electrophysiological data. Comput Intell Neurosci 2011;2011:1–9.
[46] Ortiz E, Stingl K, Münßinger J, Braun C, Preissl H, Belardinelli P. Weighted phase lag index and graph analysis: preliminary investigation of functional connectivity during resting state in children. Comput Math Methods Med 2012;2012:186353.
[47] Peng W, Hu L, Zhang Z, Hu Y. Changes of spontaneous oscillatory activity to tonic heat pain. PLoS One 2014;9:e91052.
[48] Peng W, Babiloni C, Mao Y, Hu Y. Subjective pain perception mediated by alpha rhythms. Biol Psychol 2015;109:141–50.
[49] Pfannmöller J, Strauss S, Langner I, Usichenko T, Lotze M. Investigations on maladaptive plasticity in the sensorimotor cortex of unilateral upper limb CRPS I patients. Restorative Neurol Neurosci 2019;37:143–53.
[50] Ploner M, Sorg C, Gross J. Brain rhythms of pain. Trends Cognit Sci 2017; 21:100–10.
[51] Qi R, Ke J, Schoepf UJ, Varga-Szemes A, Milliken CM, Liu C, Xu Q, Wang F, Zhang LJ, Lu GM. Topological reorganization of the default mode network in irritable bowel syndrome. Mol Neurobiol 2016;53:6585–93.
[52] Rubinov M, Sporns O. Complex network measures of brain connectivity: uses and interpretations. Neuroimage 2010;52:1059–69.
[53] Rubinov M, Kötter R, Hagmann P, Sporns O. Brain connectivity toolbox: a collection of complex network measurements and brain connectivity datasets. Neuroimage 2009;47:S169.
[54] Santarnecchi E, Galli G, Polizzotto NR, Rossi A, Rossi S. Efficiency of weak brain connections support general cognitive functioning. Hum Brain Mapp 2014;35:4566–82.
[55] Schaefer A, Kong R, Gordon EM, Laumann TO, Zuo X-N, Holmes AJ, Eickhoff SB, Yeo BT. Local-global parcellation of the human cerebral cortex from intrinsic functional connectivity MRI. Cereb Cortex 2018;28: 3095–114.
[56] Sullivan M. J., Bishop S. R., Pivik J. The pain catastrophizing scale: development and validation. Psychological assessment. 1995;7:524.
[57] Spielberger C. D. Manual for the State-Trait Anxiety Inventory (STAI). PaloAlto, CA: Consulting Psychologists Press; 1983.
[58] Sporns O, Honey CJ. Small worlds inside big brains. Proc Natl Acad Sci 2006;103:19219–20.
[59] Torta DM, Legrain V, Mouraux A, Valentini E. Attention to pain! A neurocognitive perspective on attentional modulation of pain in neuroimaging studies. Cortex 2017;89:120–34.
[60] Valentini E, Halder S, McInnerney D, Cooke J, Gyimes IL, Romei V. Assessing the specificity of the relationship between brain alpha oscillations and tonic pain. Neuroimage 2022;255:119143.
[61] van der Miesen MM, Lindquist MA, Wager TD. Neuroimaging-based biomarkers for pain: state of the field and current directions. Pain Rep 2019;4:e751.
[62] Vittersø AD, Halicka M, Buckingham G, Proulx MJ, Bultitude JH. The sensorimotor theory of pathological pain revisited. Neurosci Biobehav Rev 2022;139:104735.
[63] Wang H, Guo Y, Tu Y, Peng W, Lu X, Bi Y, Iannetti GD, Hu L. Neural processes responsible for the translation of sustained nociceptive inputs into subjective pain experience. Cereb Cortex 2023;33:634–50.
[64] Watts DJ, Strogatz SH. Collective dynamics of “small-world” networks. Nature 1998;393:440–2.
[65] Xin H, Yang B, Jia Y, Qi Q, Wang Y, Wang L, Chen X, Li F, Lu J, Chen N. Graph metrics reveal brain network topological property in neuropathic pain patients: a systematic review. J Pain Res 2024;17:3277–86.
[66] Zalesky A, Fornito A, Bullmore ET. Network-based statistic: identifying differences in brain networks. Neuroimage 2010;53:1197–207.
[67] Zalesky A, Cocchi L, Fornito A, Murray MM, Bullmore E. Connectivity differences in brain networks. Neuroimage 2012;60:1055–62.
[68] Zhang L-B, Chen Y-X, Li Z-J, Geng X-Y, Zhao X-Y, Zhang F-R, Bi Y-Z, Lu X-J, Hu L. Advances and challenges in neuroimaging-based pain biomarkers. Cell Rep Med 2024;5:101784.
[69] Zheng W, Woo CW, Yao Z, Goldstein P, Atlas LY, Roy M, Schmidt L, Krishnan A, Jepma M, Hu B, Wager TD. Pain-evoked reorganization in functional brain networks. Cereb Cortex 2020;30:2804–22.
[70] Zhu K, Chang J, Zhang S, Li Y, Zuo J, Ni H, Xie B, Yao J, Xu Z, Bian S, Yan T, Wu X, Chen S, Jin W, Wang Y, Xu P, Song P, Wu Y, Shen C, Zhu J, Yu Y, Dong F. The enhanced connectivity between the frontoparietal, somatomotor network and thalamus as the most significant network changes of chronic low back pain. Neuroimage 2024;290:120558.